Casq2 deletion causes sarcoplasmic reticulum volume increase, premature Ca^{2+} release, and catecholaminergic polymorphic ventricular tachycardia

Björn C. Knollmann,[1] Nagesh Chopra,[1] Thinn Hlaing,[2] Brandy Akin,[3] Tao Yang,[1] Kristen Ettensohn,[4] Barbara E.C. Knollmann,[5] Kenneth D. Horton,[2] Neil J. Weissman,[2] Izabela Holinstat,[1] Wei Zhang,[1] Dan M. Roden,[1] Larry R. Jones,[3] Clara Franzini-Armstrong,[6] and Karl Pfeifer[4]

[1]Oates Institute for Experimental Therapeutics and Division of Clinical Pharmacology, Departments of Medicine and Pharmacology, Vanderbilt University Medical Center, Nashville, Tennessee, USA. [2]Cardiovascular Research Institute, Washington Hospital Center, Washington, DC, USA. [3]Department of Medicine, Krannert Institute of Cardiology, Indianapolis, Indiana, USA. [4]Laboratory of Mammalian Genes and Development, National Institute of Child Health and Human Development/NIH, Bethesda, Maryland, USA. [5]Department of Pathology, Uniformed Services University of the Health Sciences, Bethesda, Maryland, USA. [6]Department of Cell and Developmental Biology, University of Pennsylvania, Philadelphia, Pennsylvania, USA.

Cardiac calsequestrin (Casq2) is thought to be the key sarcoplasmic reticulum (SR) Ca^{2+} storage protein essential for SR Ca^{2+} release in mammalian heart. Human *CASQ2* mutations are associated with catecholaminergic ventricular tachycardia. However, homozygous mutation carriers presumably lacking functional Casq2 display surprisingly normal cardiac contractility. Here we show that *Casq2*-null mice are viable and display normal SR Ca^{2+} release and contractile function under basal conditions. The mice exhibited striking increases in SR volume and near absence of the Casq2-binding proteins triadin-1 and junctin; upregulation of other Ca^{2+}-binding proteins was not apparent. Exposure to catecholamines in *Casq2*-null myocytes caused increased diastolic SR Ca^{2+} leak, resulting in premature spontaneous SR Ca^{2+} releases and triggered beats. In vivo, *Casq2*-null mice phenocopied the human arrhythmias. Thus, while the unique molecular and anatomic adaptive response to *Casq2* deletion maintains functional SR Ca^{2+} storage, lack of Casq2 also causes increased diastolic SR Ca^{2+} leak, rendering *Casq2*-null mice susceptible to catecholaminergic ventricular arrhythmias.

Introduction

Cardiac calsequestrin (Casq2), encoded by the *Casq2* gene (1, 2), is a low-affinity, high-capacity Ca^{2+}-binding protein (3, 4) located in the junctional sarcoplasmic reticulum (jSR) of mammalian myocardium (5). The jSR in heart serves as the principal site of Ca^{2+} storage and Ca^{2+} release (6). Casq2 appears as a densely staining protein in the lumen of the jSR on electron micrographs (7) and at this site forms a quaternary complex (8) with the sarcoplasmic reticulum (SR) Ca^{2+} release channel (ryanodine receptor [RyR]) and with the jSR membrane proteins triadin 1 (9) and junctin (10). Consistent with the early work on characterization of the protein in SR (3–5, 11), overexpression of cardiac Casq2 in transgenic hearts (12, 13) and in isolated cardiomyocytes (14, 15) caused massive increases in Ca^{2+} storage and release from the SR, supporting the idea that in live cardiac cells, Casq2 is the major Ca^{2+} storage protein in heart. Early observations that Casq2 binding to the RyR via triadin 1 and junctin is Ca^{2+} dependent (11) raised the possibility that Casq2 also serves as the molecular Ca^{2+} sensor that confers responsiveness of the Ryr to SR luminal Ca^{2+} (16, 17). Casq2 may also importantly regulate the development of the SR ultrastructure along with junctin and triadin 1 (18, 19). Together, these observations have suggested that Casq2 plays an essential role in the regulation of cardiomyocyte Ca^{2+} storage and release required for excitation-contraction (EC) coupling in mammalian hearts.

The importance of functional SR Ca^{2+} storage and release is demonstrated by the early embryonic lethality of mice lacking *RyR2* (20). In humans, mutations in both the *RyR2* and *CASQ2* genes have been associated with catecholaminergic polymorphic ventricular tachycardia (CPVT) and sudden cardiac death (21–25). However, unlike CPVT caused by *RyR2* mutations, CPVT linked to *CASQ2* mutations is usually autosomal recessive, and several patients homozygous for alleles predicted to entirely lack CASQ2 function have been described (22). Despite the apparent absence of CASQ2, these patients display surprisingly normal cardiac contractile function (22).

In order to determine the role of Casq2 in cardiac function and to elucidate the physiologic, molecular, and structural changes in cardiomyocytes lacking Casq2, we generated *Casq2*-null (*Casq2*$^{-/-}$) mice. Our data show that *Casq2*$^{-/-}$ mice are viable and phenocopy the human arrhythmias. Despite absent Casq2, these animals maintain relatively normal Ca^{2+} release and contractile function; we attribute this finding to unprecedented increases in SR volume, reductions in triadin 1 and junctin levels, and increased gain of Ca^{2+}-induced SR Ca^{2+} release. Significantly, while the unique molecular and anatomic adaptive response to *Casq2* deletion maintains functional SR Ca^{2+} storage, lack of Casq2 also causes increased diastolic SR Ca^{2+} leak, rendering *Casq2*$^{-/-}$ hearts susceptible to catecholaminergic ventricular arrhythmias.

Nonstandard abbreviations used: $[Ca^{2+}]_i$, intracellular $[Ca^{2+}]$; Casq2, cardiac calsequestrin; CPVT, catecholaminergic polymorphic ventricular tachycardia; EC, excitation-contraction; F_{ratio}, fluorescence ratio; jSR, junctional sarcoplasmic reticulum; PVC, premature ventricular complex; RyR, ryanodine receptor; SERCA2a, SR Ca^{2+} pump protein; SR, sarcoplasmic reticulum; TS, Tyrode solution; VT, ventricular tachycardia.

Conflict of interest: The authors have declared that no conflict of interest exists.

Citation for this article: *J. Clin. Invest.* **116**:2510–2520 (2006). doi:10.1172/JCI29128.

Figure 1
Generating the *Casq2*$^{-}$ allele. (**A**) The *Casq2* exon 1 sequence as determined by 5′ RACE. Four transcriptional starts were identified and are marked with filled arrowheads. Nucleotide number 1 represents the 5′ end of the longest identified transcript. Exon 1 includes 3 in-frame ATG translational starts (underlined). Only the second ATG is conserved in other vertebrates, and only this ATG is predicted to encode a leader sequence that would appropriately target the nascent CASQ2 peptide to the SR. (**B**) Wild-type (i) and mutant (ii) alleles of the *Casq2* locus are depicted. The *Casq2* locus spans more than 60 kb and includes 11 exons (vertical bars). Exon 1 encodes the ATG initiation codon and the first 78 amino acids. The *Casq2*$^{-}$ allele is a 1.1-kb deletion that removes 561 bp of upstream sequences, including the presumptive *Casq2* promoter (open oval) as well as the entire 431-bp exon 1 and 107 bp of intron 1.

Results

Generation of Casq2-null mice. Most *CASQ2* gene mutations found in CPVT patients described to date are predicted to induce premature stop codons (22), suggesting complete absence of CASQ2 protein in homozygous carriers. Thus, to model this genetic syndrome in mice, we wished to generate animals that were true *Casq2* nulls. Given the large size of the *Casq2* gene (11 exons spanning more than 60 kb), we reasoned that the most feasible method for generating a null allele was to delete the *Casq2* promoter and first exon. In order to deduce the location of the *Casq2* promoter, we empirically determined the 5′ boundary of exon 1 using 5′ RACE. The analyses summarized in Figure 1A show the full exon 1 sequence with its multiple transcription start sites. All identified mouse *Casq2* mRNA isoforms share 3 common in-frame ATG translational start codons, but only the second ATG is predicted to encode a peptide that would be appropriately targeted to the SR. Moreover, this is the only ATG not restricted to rodent species. Based on this information about the *Casq2* gene structure, we generated a 1.1-kb deletion that removes the entire exon 1 (with all 4 potential translational start sites) as well as 561 bp of upstream

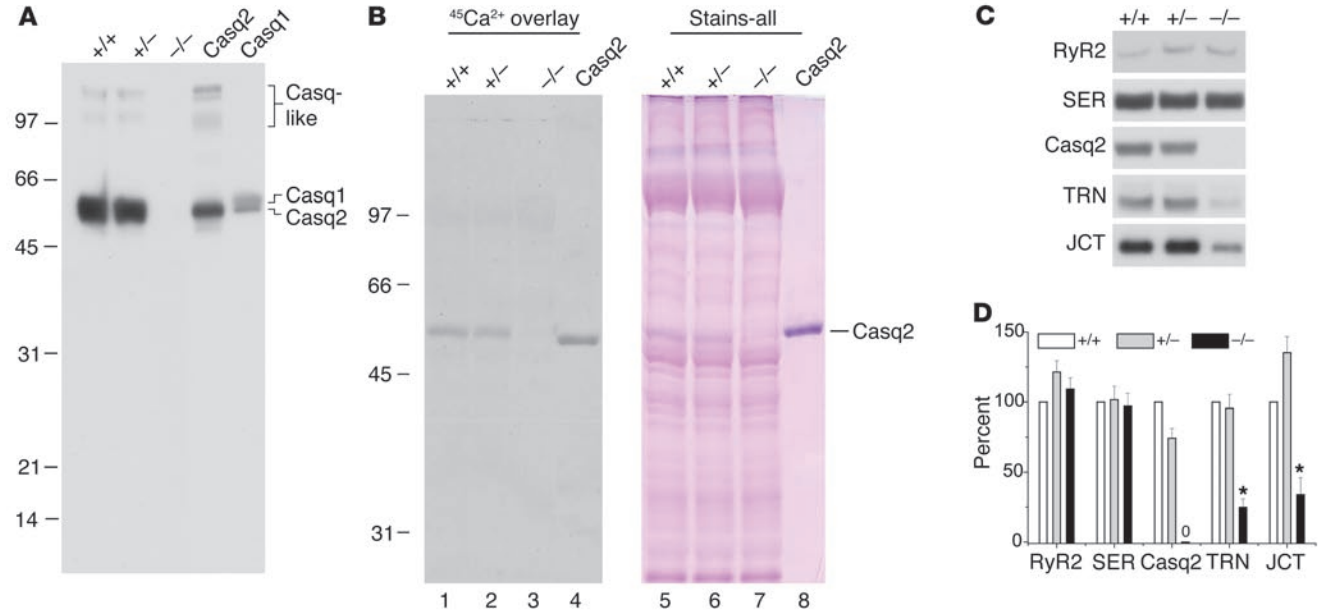

Figure 2
Casq2$^{-/-}$ hearts lack calsequestrin, display no apparent upregulation of other SR Ca^{2+}-binding proteins, and have decreased triadin 1 and junctin protein levels. (**A**) Forty micrograms of homogenate protein from *Casq2*$^{+/+}$, *Casq2*$^{+/-}$, and *Casq2*$^{-/-}$ hearts and 30 μg of microsomal protein from control membranes from mouse heart (Casq2) and skeletal muscle (Casq1) were electrophoresed per lane and probed with anti-calsequestrin antibody. Cardiac (Casq2), skeletal muscle (Casq1), and Casq-like proteins are indicated. (**B**) $^{45}Ca^{2+}$ overlay and Stains-all staining of SR membrane proteins obtained from *Casq2*$^{+/+}$, *Casq2*$^{+/-}$, and *Casq2*$^{-/-}$ hearts. Seventy-five micrograms of SR membrane protein was loaded per lane in duplicate and subjected to SDS-PAGE, then one-half of the gel was processed for $^{45}Ca^{2+}$ overlay (left) and the other half stained with Stains-all (right). One microgram of purified canine Casq2 was also run as an internal standard. (**C**) Immunoblot detection of SR proteins in microsomes isolated from 10 *Casq2*$^{+/+}$, 10 *Casq2*$^{+/-}$, and 10 *Casq2*$^{-/-}$ hearts. Forty micrograms of microsomal protein were electrophoresed per lane, transferred to nitrocellulose paper, and probed with the antibodies indicated on the left. (**D**) Quantification of protein expression levels. Data represent average values for 4 hearts per genotype expressed relative to *Casq2*$^{+/+}$ values. RyR2, cardiac isoform of the RyR; SER, SERCA2a or cardiac isoform of the Ca^{2+} pump; TRN, triadin 1 or major cardiac isoform of triadin; JCT, junctin; *$P < 0.05$.

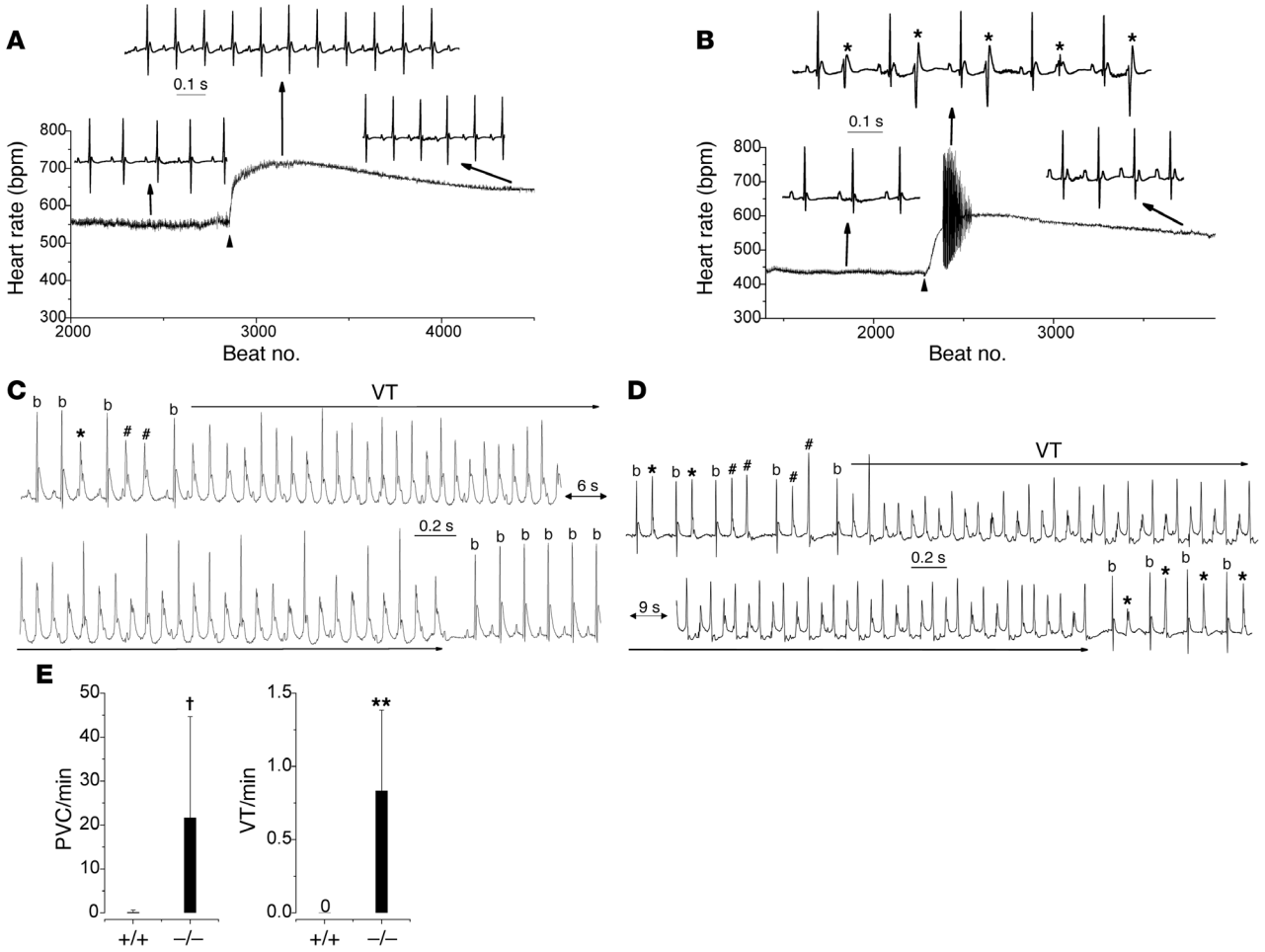

Figure 3

Casq2$^{-/-}$ mice display catecholaminergic ventricular ectopy and exercise-induced polymorphic VT. (**A** and **B**) Continuous heart rate plot and examples of surface ECG (lead 1) recordings from an anesthetized *Casq2*$^{+/+}$ (**A**) and *Casq2*$^{-/-}$ mouse (**B**) injected with the β-adrenergic receptor agonist isoproterenol (1.5 mg/kg i.p.; arrowhead). Note the multifocal PVCs (*) at the peak of the heart rate response in the *Casq2*$^{-/-}$ mouse. (**C**) Example of a telemetric ECG recording from a conscious *Casq2*$^{-/-}$ mouse obtained shortly after a treadmill exercise tolerance test. PVCs, couplets (#), and runs of polymorphic VT were frequently observed in *Casq2*$^{-/-}$ mice. All episodes of polymorphic VT reverted spontaneously back to sinus rhythm (b, sinus beat; lower record). (**D**) Example of bidirectional VT recorded in another *Casq2*$^{-/-}$ mouse. Bidirectional VT was initiated after several bigemini and couplets and terminated into stable bigemini. (**E**) Average rate of PVCs and VT episodes during a 10-minute period of post-exercise telemetric ECG recordings. $n = 5$ mice per genotype; †$P < 0.05$, **$P < 0.01$.

sequences including the presumptive *Casq2* promoter and encompassing several highly conserved DNA sequence elements. This *Casq2*$^{-}$ allele was generated as detailed in Methods and is depicted in Figure 1B. After crosses into the C57BL/6 background, mice heterozygous for the *Casq2*$^{-}$ allele were intercrossed to generate the *Casq2*$^{+/+}$ and *Casq2*$^{-/-}$ littermates used in this study. *Casq2*$^{-/-}$ mice are viable and survive into adulthood in the expected Mendelian ratios: observed/expected genotypes at weaning age were *Casq2*$^{+/+}$, 53/61; *Casq2*$^{+/-}$, 128/122; and *Casq2*$^{-/-}$, 63/61; $P = 0.5$ (χ^2).

Ablation of *Casq2* mRNA and protein in *Casq2*$^{-/-}$ hearts was confirmed by quantitative RT-PCR and Northern blot analysis (data not shown) and by immunoblot analysis, which was unable to detect any Casq2 protein in *Casq2*$^{-/-}$ mice (Figure 2A); thus the gene does not use any downstream start sites. The previously described high-molecular-weight "calsequestrin-like proteins" (3), presumed polymers of Casq2 present in low content that cross-react with anti-calsequestrin antibodies (26), were also completely ablated from *Casq2*$^{-/-}$ hearts (Figure 2A). Skeletal muscle calsequestrin (*Casq1*), the other calsequestrin isoform, which is not normally expressed in mammalian ventricle (2), could potentially substitute for cardiac *Casq2*. However, we found that Casq1 was not detectable in *Casq2*$^{-/-}$ hearts at the mRNA (data not shown) or protein level (Figure 2A).

$^{45}Ca^{2+}$ overlay (11) and Stains-all staining (5) were used to further verify the total absence of calsequestrin in SR vesicles from *Casq2*$^{-/-}$ hearts (Figure 2B). As shown previously (11) by the $^{45}Ca^{2+}$ overlay method, Casq2 is the major Ca^{2+}-binding protein in cardiac SR vesicles, and this was confirmed for SR vesicles isolated from both *Casq2*$^{+/+}$ and *Casq2*$^{+/-}$ mice (Figure 2B, lanes 1 and 2). In contrast, no significant $^{45}Ca^{2+}$-binding protein was detected in membranes from *Casq2*$^{-/-}$ mice (lane 3). Likewise, Stains-all staining revealed that the major blue-staining, 55-kDa protein band

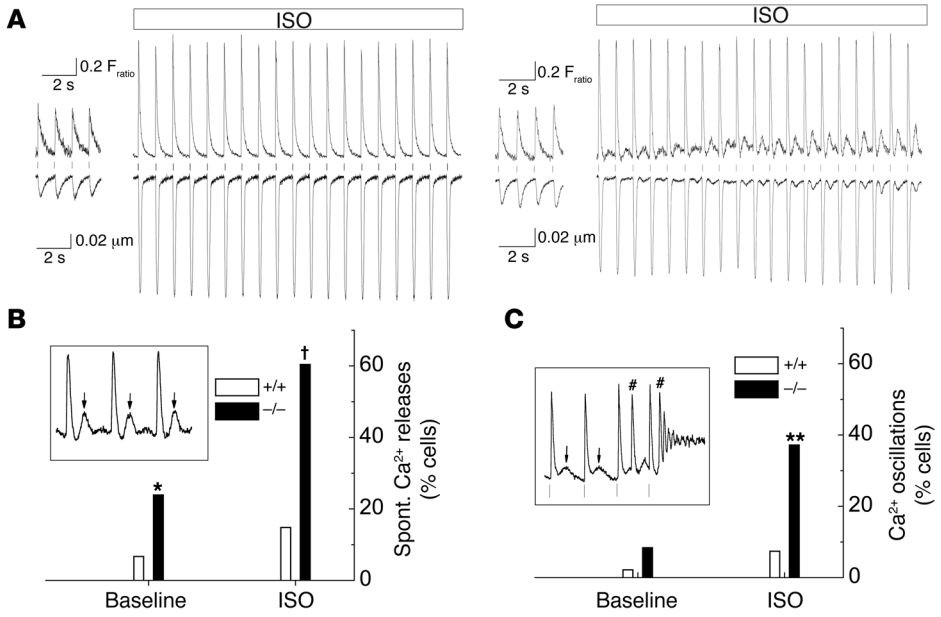

Figure 4

Casq2$^{-/-}$ myocytes display spontaneous Ca^{2+} releases and triggered beats but largely maintain normal contractility, SR Ca^{2+} release amplitudes, and SR Ca^{2+} content. (**A**) Examples of $[Ca^{2+}]_i$ transients (top traces) and cell shortening (bottom traces) recorded from fura-2/AM–loaded, field-stimulated myocytes (1 Hz). Application of 1 μmol/l isoproterenol (ISO) significantly increased Ca^{2+} transients and cell shortening in both myocytes. Note that shortly after ISO application was started, only the *Casq2*$^{-/-}$ myocyte displayed spontaneous Ca^{2+} releases and aftercontractions of increasing amplitude following each paced twitch (vertical lines). (**B** and **C**) Comparison of the incidence of spontaneous (Spont.) Ca^{2+} release events (**B**) and Ca^{2+} oscillations (**C**) at baseline and in the presence of ISO. Data represent the fraction (%) of myocytes that displayed at least 1 event during a 20-second recording period. Insets show representative examples of spontaneous Ca^{2+} after-releases (arrows in **B**, inset) and Ca^{2+} oscillations (**C**, inset) induced by spontaneous Ca^{2+} releases and triggered beats (# in **C**, inset). $^*P < 0.05$, $^{**}P < 0.01$, $^{\dagger}P < 0.001$, *Casq2*$^{-/-}$ versus *Casq2*$^{+/+}$ myocytes by Fisher's exact test. *Casq2*$^{+/+}$ myocytes: $n = 45$ (baseline) and 27 (ISO); *Casq2*$^{-/-}$ myocytes: $n = 71$ (baseline) and 43 (ISO).

corresponding to Casq2 (3–5) was entirely absent from cardiac SR vesicles isolated from *Casq2*$^{-/-}$ hearts (Figure 2B, lane 7). In sum, the *Casq2*$^{-}$ allele is a true null and results in complete loss of Casq2 without compensation by upregulation of Casq1 or of other obvious Ca^{2+}-binding proteins. Thus, calsequestrin expression in the heart is not required for viability.

We next examined expression levels of proteins normally associated with Casq2 in the SR. Protein levels of cardiac RyRs (RyR2) were unchanged in *Casq2*$^{-/-}$ hearts (Figure 2, C and D). However, levels of the calsequestrin-binding proteins triadin 1 and junctin were substantially downregulated (Figure 2, C and D). By comparison, the level of the SR Ca^{2+} pump protein (SERCA2a), found predominantly in the free SR (5), was unchanged (Figure 2, C and D). Thus, the physiological changes of *Casq2*$^{-/-}$ mice described below should be considered in the context of the rather drastic downregulation of Casq2's 2 partner proteins, triadin 1 and junctin.

Surface ECG and echocardiographic measurements were obtained to determine the effect of *Casq2* ablation on cardiac function in vivo. Similar to human homozygous carriers of *CASQ2* mutations (21, 22), *Casq2*$^{-/-}$ mice displayed a significantly slower heart rate but normal cardiac contractility, normal left-ventricular cavity size, and unchanged ECG parameters (Supplemental Table 1; supplemental material available online with this article; doi:10.1172/JCI29128DS1). Systolic blood pressure measured using tail-cuff method was not statistically different between the 2 groups (*Casq2*$^{+/+}$: 106 ± 18 mmHg, $n = 7$; *Casq2*$^{-/-}$: 99 ± 20 mmHg, $n = 5$; $P = 0.53$). *Casq2*$^{-/-}$ mice had a modest but statistically significant increase in ventricular wall thickness (Supplemental Table 1) and an approximately 10% increase in heart to body weight ratio (*Casq2*$^{+/+}$: 6.3 ± 0.6 mg/g, $n = 5$; *Casq2*$^{-/-}$: 7.0 ± 1.12 mg/g, $n = 6$; $P < 0.05$). Histological examination of mouse hearts demonstrated that this was not associated with significant ventricular fibrosis or myofibrillar disarray (Supplemental Figure 2).

Casq2$^{-/-}$ *mice display CPVT.* After catecholamine challenge with the β-adrenergic agonist isoproterenol, anesthetized *Casq2*$^{-/-}$ mice displayed frequent multifocal premature ventricular complexes (PVCs), which occurred during the time of maximum heart rate response (Figure 3B). *Casq2*$^{-/-}$ mice had on average 2.1 ± 2.53 PVCs/min ($n = 11$), whereas PVCs were rare, isolated events in *Casq2*$^{+/+}$ mice (0.07 ± 0.1 PVCs/min; $n = 16$; $P < 0.05$). Polymorphic nonsustained ventricular tachycardia (VT) occurred in 3 of 11 *Casq2*$^{-/-}$ mice but was not observed in *Casq2*$^{+/+}$ mice. The coupling intervals of the PVCs were long, with a ratio of 0.86 ± 0.071 (range 0.56–0.96; $n = 51$) relative to the preceding RR interval. A predominance of long-coupled PVCs has also been described in CPVT patients (27).

We next subjected the mice to treadmill exercise while continuously monitoring the ECG by telemetry. Maximum running time on the treadmill was not statistically different between the 2 groups of mice (*Casq2*$^{+/+}$: 8.2 ± 1.3 min, $n = 5$; *Casq2*$^{-/-}$: 6.8 ± 2.4 min, $n = 5$; $P = 0.35$). Unlike *Casq2*$^{+/+}$ mice, *Casq2*$^{-/-}$ mice developed multiple episodes of ventricular bigeminy, couplets (2 successive PVCs), and polymorphic VT after the exercise test (Figure 3C). Interestingly, the polymorphic VT frequently displayed an alternating QRS complex (Figure 3D) consistent with bidirectional VT, which is characteristic of CPVT patients (24, 28). Figure 3E compares the rate of exercise-induced PVCs and VT between *Casq2*$^{+/+}$ and *Casq2*$^{-/-}$ mice. Interestingly, the frequency of PVCs and VT episodes was significantly higher in conscious *Casq2*$^{-/-}$ mice after exercise (22 ± 22.5 PVCs/min; Figure 3E) compared with anesthetized *Casq2*$^{-/-}$ mice after catecholamine challenge ($P < 0.001$), suggesting that anesthesia suppressed the rate of ventricular arrhythmias. In total, 56 episodes of VT (duration ranging from 0.5 seconds to 145 seconds) were observed in 5 mice during the 10-minute recording period following the exercise stress, while VT did not occur in the 5 *Casq2*$^{+/+}$ mice tested (Figure 3E; $P < 0.01$).

Casq2 ablation causes spontaneous SR Ca^{2+} *releases and triggered beats in cardiomyocytes.* To begin investigating the cellular mechanism for the catecholaminergic ventricular arrhythmias observed in

Table 1
$[Ca^{2+}]_i$ and sarcomere shortening measurements in ventricular myocytes

	Baseline		Isoproterenol	
	Casq2$^{+/+}$ (*n* = 28)	*Casq2*$^{-/-}$ (*n* = 47)	*Casq2*$^{+/+}$ (*n* = 18)	*Casq2*$^{-/-}$ (*n* = 20)
Ca^{2+} transient				
Diastolic signal (F_{ratio})	1.50 ± 0.17	1.70 ± 0.24[A]	1.49 ± 0.16	1.67 ± 0.22[A]
Peak height (F_{ratio})	0.73 ± 0.36	0.72 ± 0.37	1.73 ± 0.57	1.37 ± 0.57
Time to peak (ms)	39.0 ± 12.0	52.0 ± 19.7[A]	40.0 ± 16.8	41.0 ± 20.2
Time to 50% peak (ms)	15.0 ± 3.6	19.0 ± 6.2[A]	11.0 ± 2.2	15.0 ± 5.7[A]
τ (ms)	256 ± 94	250 ± 88	97 ± 38	96 ± 57
Time to 90% relaxation (ms)	527 ± 135	494 ± 150	232 ± 111	240 ± 119
Cell shortening				
Diastolic SL (μm)	1.80 ± 0.062	1.79 ± 0.058	1.74 ± 0.09	1.73 ± 0.16
% FS	2.68 ± 2.39	2.80 ± 2.86	10.0 ± 6.23	12.4 ± 23.19
Time to peak (ms)	172 ± 45.2	185 ± 42.8	140.0 ± 20.9	179 ± 163
Time to 50% peak (ms)	68 ± 13	80 ± 17.7[A]	51.0 ± 5.3	72.0 ± 29.5[A]
Time to 90% relaxation (ms)	435 ± 29	374 ± 20	216 ± 62.0	219 ± 34.0

Diastolic signal: F_{ratio} immediately prior to paced beat; Peak height: difference between diastolic F_{ratio} and F_{ratio} at peak Ca^{2+} transient; Time to 50% peak: time from onset to 50% peak Ca^{2+}/cell shortening; Time to 90% relaxation: Time from peak Ca^{2+}/cell shortening to 90% decline; τ: time constant of the Ca^{2+} transient decay obtained by monoexponential curve fit; Diastolic segment length (SL): average distance between discrete striations of the cardiomyocyte using power spectrum analysis software (IonWizard; IonOptix); % FS: ratio of absolute cell shortening amplitude to diastolic cell length. [A]$P < 0.05$ compared with *Casq2*$^{+/+}$.

vivo (Figure 3), we next measured intracellular $[Ca^{2+}]$ ($[Ca^{2+}]_i$) and cell shortening in isolated, field-stimulated myocytes loaded with the fluorescent Ca^{2+} indicator fura-2. Representative tracings are depicted in Figure 4. *Casq2*$^{-/-}$ myocytes frequently developed transient rises in diastolic Ca^{2+} and aftercontractions following each paced beat (Figure 4A). These spontaneous premature Ca^{2+} release events occurred in a statistically significant larger fraction of *Casq2*$^{-/-}$ cells compared with *Casq2*$^{+/+}$ myocytes even under basal conditions, but the difference in frequencies was particularly striking when cells were exposed to isoproterenol (Figure 4, A and B). Such slow and low-level Ca^{2+} transients are reminiscent of spontaneous SR Ca^{2+} release events and Ca^{2+} waves typically observed under SR Ca^{2+} overload conditions (29) or in myocytes transiently transfected with CPVT-linked *Casq2* mutants (23). Consistent with this idea, application of caffeine, which opens RyRs and empties the SR (30), completely abolished the aftercontractions and spontaneous Ca^{2+} transients (data not shown). The spontaneous Ca^{2+} releases triggered full-fledged beats, resulting in sustained Ca^{2+} oscillations significantly more often in *Casq2*$^{-/-}$ compared with *Casq2*$^{+/+}$ myocytes (Figure 4C). Together, these data strongly support the idea that premature SR Ca^{2+} release events causing delayed afterdepolarizations and triggered beats are responsible for the ventricular ectopy and CPVT observed in vivo.

Casq2 ablation has little effect on SR Ca^{2+} release, myocyte contractility, and SR Ca^{2+} content in basal conditions but significantly increases SR Ca^{2+} leak during isoproterenol exposure. Although we identified abnormal spontaneous Ca^{2+} release events in *Casq2*$^{-/-}$ cells, it is equally noteworthy that field-stimulated Ca^{2+} transients and cell shortening were surprisingly normal in *Casq2*$^{-/-}$ myocytes (Figure 4A). Indeed, twitch Ca^{2+} transient amplitude, Ca^{2+} transient decay kinetics, myocyte diastolic sarcomere length, and myocyte shortening and relaxation were not significantly different between the 2 groups of myocytes (Table 1). Even in the presence of isoproterenol, Ca^{2+} transients and cell shortening parameters remained largely intact (Table 1). These results are consistent with the normal contractility of *Casq2*$^{-/-}$ mice measured in vivo (compare Supplemental Table 1) but surprising given the complete loss of the major SR Ca^{2+} storage protein in *Casq2*$^{-/-}$ myocytes. To assess the effect of *Casq2* ablation on SR Ca^{2+} storage capacity, total SR Ca^{2+} content was measured by rapid application of caffeine (Figure 5A). SR Ca^{2+} content of *Casq2*$^{-/-}$ myocytes was only decreased by 11% in basal conditions but decreased more significantly (30%) in the presence of isoproterenol (Figure 5B, left panel). Na/Ca exchanger function was estimated by the decay of cytosolic Ca^{2+} during caffeine application (31) and was not significantly different between the 2 groups (time to 50% relaxation of caffeine transient: *Casq2*$^{+/+}$, 1.30 ± 0.70 s, $n = 40$; *Casq2*$^{-/-}$, 1.26 ± 0.59 s, $n = 67$; $P = 0.72$). Basal and isoproterenol-stimulated L-type Ca^{2+} current was also not significantly different between the 2 groups of myocytes (Supplemental Figure 3). On the other hand, the fraction of total SR Ca^{2+} released during each beat was significantly increased in *Casq2*$^{-/-}$ myocytes (Figure 5B, right panel). Together these data suggest that loss of Casq2 sensitizes the RyR2 channel complex to activation by Ca^{2+}, resulting in increased gain of SR Ca^{2+} release during EC coupling. While this increased EC coupling gain likely contributed to maintaining normal twitch Ca^{2+} transients and contractile function in *Casq2*$^{-/-}$ myocytes, sensitization of the RyR2 channel likely would lead to increased SR Ca^{2+} loss via the RyR2 channel during diastole (SR Ca^{2+} leak). Indeed, we found that in the presence of isoproterenol, SR Ca^{2+} leak was significantly increased in *Casq2*$^{-/-}$ myocytes (Figure 5, C and D). Conversely, when SR Ca^{2+} leak was prevented by application of tetracaine, SR Ca^{2+} content was not statistically different between the 2 groups (Figure 5D, right panel). In normal myocytes, SR Ca^{2+} leak increases exponentially with increased SR Ca^{2+} load (32). Loss of Casq2 in *Casq2*$^{-/-}$ myocytes did not change this fundamental relationship but rather shifted the leak-load curve leftward compared with that of *Casq2*$^{+/+}$ myocytes (Figure 5E).

Casq2 ablation increases SR volume and surface area. While the above-described findings provide a good explanation for the maintained contractility and increased rate of diastolic SR Ca^{2+} release, they cannot account for the normal SR Ca^{2+} storage capacity of *Casq2*$^{-/-}$ myocytes. Thus, we next investigated the SR ultrastructure of *Casq2*$^{-/-}$ hearts. In *Casq2*$^{+/+}$ mice, calsequestrin is located within the flat cisternae of the jSR that are associated either with the transverse tubules, forming dyads (Figure 6, A and B, between arrows), or with the surface membrane, forming peripheral couplings. Within the jSR, calsequestrin is condensed into periodic clumps, a structural disposition that is induced by the attachment of calsequestrin to the jSR membrane proteins triadin 1 and junctin (18, 19). Small densities, or "feet," constituted by the cytoplasmic domains of RyRs separate the adjacent SR and

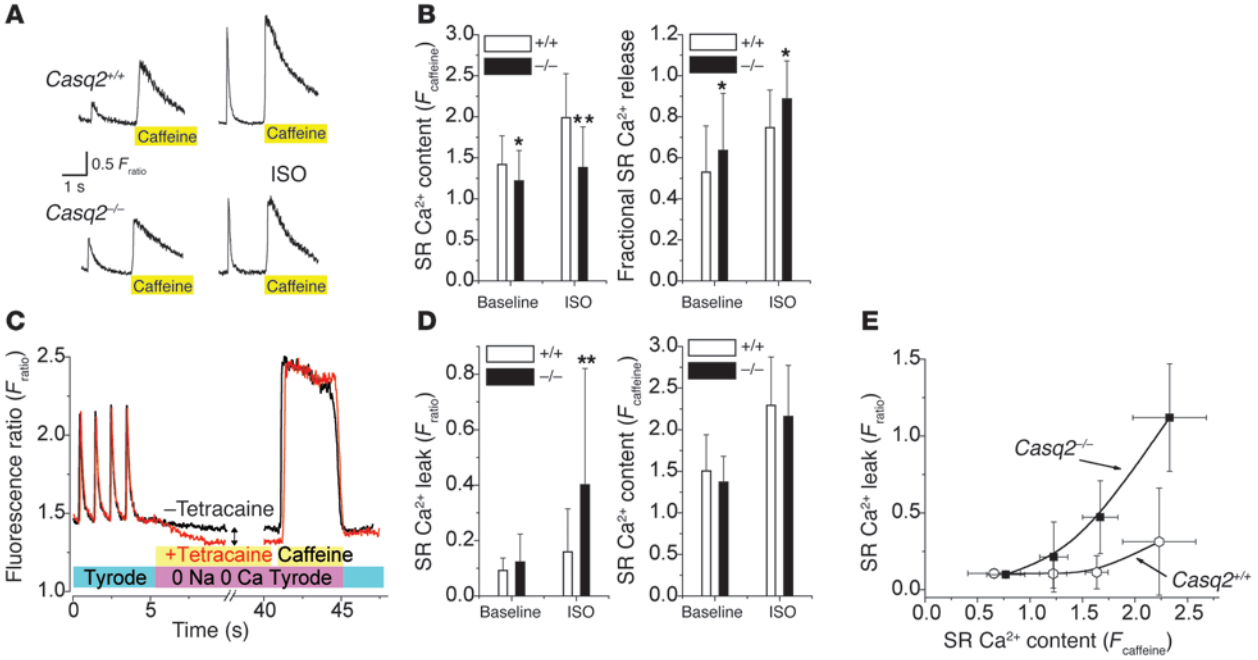

Figure 5

Casq2$^{-/-}$ myocytes have largely preserved SR Ca^{2+} release and SR Ca^{2+} content under basal conditions, but isoproterenol application causes increased SR Ca^{2+} leak. (**A**) Representative examples of rapid application of caffeine (10 mmol/l) to a *Casq2*$^{+/+}$ (top) and a *Casq2*$^{-/-}$ myocyte (bottom). Myocytes were field stimulated at 1 Hz to maintain consistent SR Ca^{2+} load. Note the increased twitch transient and caffeine-induced transients in the presence of ISO (1 μmol/l; right). The height of the caffeine-induced Ca^{2+} transient was used as a measure of total SR Ca^{2+} content (30). Fractional SR Ca^{2+} release was calculated by dividing the height of the last twitch transient by the height of the caffeine transient. (**B**) Comparison of average SR Ca^{2+} content (left) and fractional SR Ca^{2+} release (right). *$P < 0.05$, **$P < 0.01$. *Casq2*$^{+/+}$ myocytes: $n = 41$ (baseline) and 27 (ISO); *Casq2*$^{-/-}$ myocytes: $n = 70$ (baseline) and 37 (ISO). (**C**) Protocol used to measure SR Ca^{2+} leak as described in ref. 32. Plasma membrane Ca^{2+} flux is eliminated by removal of extracellular Na^+ and Ca^{2+}. The drop in steady-state $[Ca^{2+}]_i$ (double arrow) represents a shift of Ca^{2+} from the cytosol to the SR when RyR2 channels are inhibited by tetracaine (1 mmol/l) and was used as a measure of SR Ca^{2+} leak. (**D**) Comparison of average SR Ca^{2+} leak (left) and SR Ca^{2+} content in the presence of tetracaine (right). Note that when SR Ca^{2+} leak was blocked by tetracaine, SR Ca^{2+} content was not significantly different between the 2 groups. **$P < 0.01$. *Casq2*$^{+/+}$ myocytes: $n = 32$ (baseline) and 45 (ISO); *Casq2*$^{-/-}$ myocytes: $n = 29$ (baseline) and 42 (ISO). (**E**) SR Ca^{2+} leak in the presence of ISO plotted as a function of SR Ca^{2+} content. Note that the SR Ca^{2+} leak of *Casq2*$^{-/-}$ myocytes remained SR load dependent but was shifted to the left compared with that of *Casq2*$^{+/+}$ myocytes.

T tubule membranes. Lack of calsequestrin, junctin, and triadin 1 in *Casq2*$^{-/-}$ myocardium did not affect the docking of jSR to T tubules (Figure 6, C–E) and to the surface membrane (Figure 6F), but it did produce distinct changes in the jSR cisternae. The cisternae appeared empty and their size was more variable, being either slightly narrower (Figure 6, C and D) or noticeably wider (Figure 6, E and F) than in wild-type myocardium. In some cisternae (e.g., Figure 6E), a very diffuse density was present in the SR, but it appeared quite different from the condensed calsequestrin of *Casq2*$^{+/+}$ SR (compare with Figure 6A).

The free SR forms a continuous network over the middle of the sarcomere and is connected to the flat jSR cisternae in proximity of the Z lines, where the T tubules are located. Figure 6G shows a view of the SR in a *Casq2*$^{-/-}$ myocyte. Its general disposition was not different from that found in *Casq2*$^{+/+}$ myocytes, but the frequency of SR tubular profiles was higher than usual. This was confirmed by morphometric analysis comparing the surface density and volume fraction of SR membranes in *Casq2*$^{+/+}$ and *Casq2*$^{-/-}$ left-ventricular myocardium (Table 2). SR volume related either to total cytoplasmic volumes or to myofibrillar volumes increases by approximately 51% and 45%, respectively, in *Casq2*$^{-/-}$ hearts. SR surface areas related to total and myofibrillar volumes show an increase of approximately 52% and 49%, respectively. The differences were highly significant ($P < 10^{-13}$ to 10^{-21}). In contrast, mitochondria occupied an almost identical fraction of the cell volume in both groups of myocytes (Table 2).

Discussion

Comprehensive evaluation of cardiac function and structure in the *Casq2*$^{-/-}$ mice has generated important new insights regarding the function of Casq2. First, Casq2 is not essential for providing sufficient Ca^{2+} storage for normal function of cardiac muscle. This is a surprising finding, since Casq2 is by far the most abundant SR Ca^{2+}-binding protein (11, 30). A highly significant increase (~50%) in SR volume is apparently sufficient to maintain near normal SR Ca^{2+} storage capacity in Casq2-deficient mice. Interestingly, SERCA2a expression levels were unchanged, suggesting that SERCA2a density in the SR membrane is decreased by approximately 50% (compare Figure 2B and Table 2). The relative abundance of SR increases during early postnatal myocardium differentiation but then remains constant throughout adulthood (33). Heart hypertrophy-inducing challenges result in an overall increase in cell volume but do not change the SR/myofibril ratio (34). Thus, the SR expansion in response to lack of

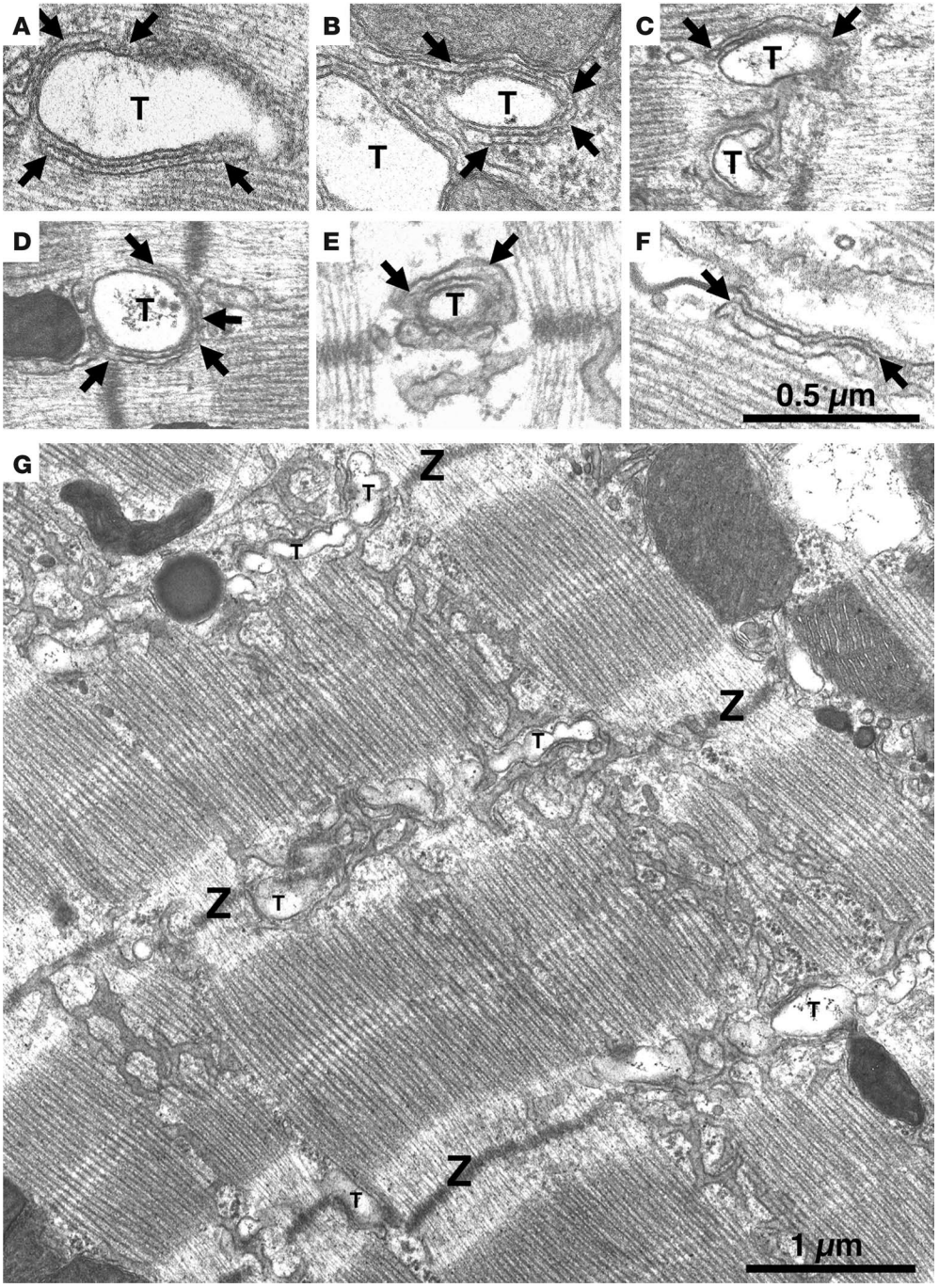

Figure 6
jSR lacks its visible content, and overall SR volume is increased in *Casq2*$^{-/-}$ ventricular myocytes. Electron micrographs of left-ventricular myocytes from *Casq2*$^{+/+}$ (**A** and **B**) and *Casq2*$^{-/-}$ (**C**–**G**) hearts. Flat jSR cisternae are closely apposed to T tubules (T). In *Casq2*$^{+/+}$ myocytes, cisternae are quite uniform in width and filled by calsequestrin, which is periodically arranged in small clumps (**A** and **B**, between arrows). "Feet" (RyRs) are present in the junctional gap between the 2 membranes. In *Casq2*$^{-/-}$ myocytes, the jSR has variable width and is apparently empty (**C**–**F**, between arrows). (**G**) Longitudinal SR of a *Casq2*$^{-/-}$ myocyte in a section that was cut tangentially to the myofibrils. The SR forms a network with large fenestrations covering the A bands and continuing across Z lines (Z). In proximity to the T tubules, the SR runs in a transverse orientation, accompanying the T tubule profiles. The SR network is quite abundant in *Casq2*$^{-/-}$ myocytes (see data in Table 2).

Casq2 is unprecedented. We speculate that a similar SR volume increase occurs in human carriers of *CASQ2* nonsense mutations, which would explain why cardiac contractility is normal in patients presumably lacking Casq2 protein (22).

Second, Casq2 importantly modulates SR Ca^{2+} release but is not required for luminal SR Ca^{2+} sensing. We find that even in the absence of Casq2, SR Ca^{2+} leak remains steeply nonlinear with increasing SR Ca^{2+} content. This is somewhat of a surprise, since studies have suggested that Casq2 together with triadin 1 and junctin serves as the luminal Ca^{2+} sensor that dynamically regulates the RyR2 open probability (16, 17). We discovered that the highly homologous skeletal muscle Casq1 is also not expressed in *Casq2*$^{-/-}$ mice. Hence, the RyR2 channel can sense luminal Ca^{2+} even in the absence of calsequestrin, possibly via a cytoplasmic site, as suggested by earlier studies (35). Rather, Casq2 appears to function as a modulator of SR Ca^{2+} release that shifts the leak-load relationship to the right and reduces SR Ca^{2+} leak and therefore RyR2 open probability in conditions of high SR Ca^{2+} load, reminiscent of the RyR2 regulation by calstabin2 (36) or calcium/calmodulin-dependent kinase II (CaMKII) (37). This idea is consistent with the observations that Ca^{2+}-induced Ca^{2+} release and EC coupling gain are profoundly decreased in myocytes overexpressing Casq2 either acutely (15) or chronically (12, 38). Furthermore,

Table 2
Total SR volume and surface area in left-ventricular myocytes

	Casq2$^{+/+}$	*Casq2*$^{-/-}$	*P*
Mitochondrial vol/total vol (%)	37.1 ± 6.86	34.1 ± 5.78	[A]
SR volume/total vol (%)	1.42 ± 0.81	2.14 ± 0.81	1.3×10^{-15}
SR volume/cytopl. vol (%)	2.27 ± 0.87	3.30 ± 1.27	1.5×10^{-13}
SR surface area/total vol ($\mu m^2/\mu m^3$)	0.65 ± 0.22	0.99 ± 0.28	1.4×10^{-21}
SR surface area/cytopl. vol ($\mu m^2/\mu m^3$)	1.03 ± 0.34	1.53 ± 0.43	2.1×10^{-14}

The first row gives the mitochondrial volume in relation to the myocyte volume (excluding nuclei and Golgi regions). This volume was subtracted from the total volume to yield the cytoplasmic (cytopl.) volume. The second and third rows give the SR volume in relation to the total and the cytoplasmic volumes, respectively. The fourth and fifth rows give SR surface area in relation to the total and the cytoplasmic volumes, respectively. *n* = 135–136 micrographs, from 45–47 cells, 3 mice per group. [A]The slightly larger mitochondrial volume in *Casq2*$^{+/+}$ cells was due to the fact that in one *Casq2*$^{+/+}$ myocardium, the mitochondria were dilated due to a fixation artifact.

acute reductions in Casq2 in isolated myocytes increased the frequency of diastolic SR Ca^{2+} release (14). Almost complete downregulation of triadin 1 and junctin (Figure 2) may help maintain RyR2 function in *Casq2*$^{-/-}$ mice, since triadin 1 and/or junctin in the absence of Casq2 (17) or excess triadin 1 in the presence of Casq2 (39) appear to increase EC coupling gain and/or RyR2 open probability.

Third, our data directly demonstrate the mechanism underlying cardiac arrhythmias associated with *CASQ2* mutations: Lack of calsequestrin in *Casq2*$^{-/-}$ myocytes causes premature spontaneous SR Ca^{2+} releases and triggered beats, resulting in arrhythmias in *Casq2*$^{-/-}$ mice that phenocopy the catecholaminergic ventricular arrhythmias observed in their human counterparts (21, 22). Previous in vitro experiments with transfected isolated myocytes that achieved only a reduction but not ablation of endogenous Casq2 (14) also indicated that a decrease in Casq2 can lead to spontaneous SR Ca^{2+} release. Interestingly, *RyR2* mutations linked to the CPVT syndrome also appear to sensitize the RyR2 to Ca^{2+}, resulting in enhanced store overload–induced Ca^{2+} release events (40–42). Alternatively, the RyR2 mutations may interfere with calstabin2 (FKBP12.6) binding to RyR2, resulting in "leaky" RyR2 channels (43, 44). Our finding of increased diastolic SR Ca^{2+} leak in *Casq2*$^{-/-}$ myocytes after isoproterenol application suggests that either Casq2 modulates RyR2 channels in a fashion similar to calstabin2 or that loss of Casq2 enhances unbinding of calstabin2 from the RyR2 channel complex during β-adrenergic stimulation (36).

Fourth, our data indicate that calsequestrin is responsible for the electron-dense "clumps" of the SR cisternae observed on electron micrographs, as initially suggested for skeletal muscle (45). In addition and more importantly, we demonstrate that Casq2, junctin, and triadin 1 are not required either for the docking of jSR to T tubule/surface membrane or for the dihydropyridine receptor–RyR association at the docking sites that is responsible for EC coupling. These findings extend our previous observations that junctin (and also presumably triadin 1) become associated with dyads and peripheral couplings only after the junctions are formed during normal cardiac myocyte differentiation (18, 19).

Fifth, Casq2 is required to maintain triadin 1 and junctin protein levels. This appears to be a direct effect of Casq2 on triadin 1 and junctin protein synthesis and/or stability, since junctin and triadin 1 mRNA levels remained unchanged in *Casq2*$^{+/+}$ mice (unpublished observations). Future studies will be needed to further examine the mechanism responsible for this phenomenon.

Finally, our data demonstrate that Casq2 protein levels of heterozygote *Casq2*$^{+/-}$ hearts were only modestly decreased (~25%) and triadin 1 and junctin protein levels were essentially unchanged. These data may explain why heterozygous carriers of *Casq2* mutations are either asymptomatic or significantly less symptomatic compared with homozygous patients (21–23).

There are a number of caveats to consider when applying the results of our experiments to human biology: While conscious *Casq2*$^{-/-}$ mice had numerous episodes of polymorphic and bidirectional VT, the VT did not degenerate into ventricular fibrillation, and sudden cardiac deaths were also not observed. This contrasts with reports in humans, where sudden death is one of the hallmarks of this disease (22, 28, 44). A likely contributor is that mice are generally less susceptible to ventricular tachyarrhythmias than larger species because of their small ventricular mass (46).

Casq2$^{-/-}$ mice had a slight increase in heart weight and left-ventricular wall thickness (Supplemental Table 1), whereas patients with CASQ2 mutations had no structural heart disease by echocardiography (22). While we do not have an explanation for this discrepancy, the number of clinical cases with *CASQ2* mutations is extremely small, and echocardiography was not done in matched control patients. As a result, a mild ventricular hypertrophy could have been missed. On the other hand, the hypertrophic response observed in *Casq2*$^{-/-}$ mice may represent a species difference resulting from the greater reliance of murine cardiac muscle on SR Ca^{2+} release and storage (~90% per beat) compared with that in larger mammals including humans (~65%) (6). Although the *Casq2*$^{-/-}$ cardiomyocytes had near normal Ca^{2+} transient amplitudes and SR Ca^{2+} stores (Figure 5), rates of Ca^{2+} release and cell shortening were modestly (10%–25%) but nevertheless significantly slower (Table 1). These data suggest that either it takes longer to mobilize the Ca^{2+} from the larger nonjunctional SR network (Figure 6G) to the junctional SR or that local SR Ca^{2+} release termination is slowed in myocytes lacking Casq2. This may have contributed to a less efficient EC coupling process and compensatory cardiac hypertrophy.

Compensatory mechanisms other than the expansion of SR volume and downregulation of triadin 1 and junctin may have occurred in *Casq2*$^{-/-}$ mice and helped maintain SR Ca^{2+} storage. While we cannot exclude upregulation of other Ca^{2+}-binding proteins, the Stains-all staining and $^{45}Ca^{2+}$ overlay experiments (Figure 2B) demonstrated that no other Ca-binding proteins such as calreticulin are upregulated to an extent that could compensate for the loss of Casq2. Consistent with this apparent lack of significant upregulation of other SR Ca^{2+}-buffering proteins, the observed expansion of SR volume by 50% is predicted to almost fully compensate for the loss of SR Ca^{2+} buffering by Casq2, based on estimates that Casq2 binds approximately 50% of the total Ca^{2+} stored in the SR (47). As a result, the free SR Ca^{2+} concentration may change very little or not at all in *Casq2*$^{-/-}$ myocytes. This may explain why Ca^{2+} transient decay kinetics (largely a function of SR Ca^{2+} uptake by SERCA2a; ref. 31) remained unchanged, even though the SERCA2a density in the SR membrane was decreased by approximately 50% in *Casq2*$^{-/-}$ myocytes.

In summary, our results indicate that Casq2 is not essential for cardiac Ca^{2+} storage, which can be maintained an expansion of SR volume that has not to our knowledge been previously reported.

Rather, Casq2's primary function apparently is that of an inhibitory modulator of the RyR2 channel complex during conditions of high SR Ca^{2+} load and/or β-adrenergic stimulation. As a result, functional Casq2 is required to prevent premature spontaneous SR Ca^{2+} releases and thus to maintain an orderly heart rhythm during adrenergic stimulation such as the fight-or-flight response.

Methods

Generating the Casq2^{-} allele

All studies were approved by the institutional animal care and use committees at the NIH intramural program, Georgetown University, and Vanderbilt University and performed in accordance with NIH guidelines. To generate the *Casq2*$^{-}$ allele, sequences between –561 and +538 were replaced with a small insertion of about 80 bp that includes a single *loxP* element. (Note that all bases are numbered relative the *Casq2* transcription start site nearest the 5′ end, as depicted in Figure 1A). This allele was generated in a multistep process. For maps and further details, see Supplemental Methods and Supplemental Figure 1. In step 1, mouse embryonic stem cells (RI line, 129SV) were transformed with linearized plasmid pKP588. pKP588 includes a 2.1-kb 5′ homology flank and a 2.0-kb 3′ homology flank to direct insertion of a 30-bp element carrying a loxP element at –561 bp and a 2.1 kb *NeoR* cassette at +538 bp inside intron 1. (The *NeoR* cassette carried 2 flanking *Frt* elements as well as single *loxP* site). pKP588 also carries a 3.0-kb *Diphtheria toxin A* gene for negative selection. G418-resistant colonies were isolated and scored for homologous integration by PCR amplification using 1 primer from outside the flanking sequences included in plasmid pKP588 and 1 primer internal to the *NeoR* cassette. Targeted clones were injected into C57BL/6 blastocysts and chimeric founder mice crossed with C57BL/6 females to establish the *Casq2*$^{floxed+Neo}$ line. In step 2, *Casq2*$^{floxed+Neo}$ heterozygotes were crossed to *Rosa26-Flp* transgenic females (strain 003946; The Jackson Laboratory) to remove the *NeoR* cassette via Flip recombinase–mediated site-specific recombination. The *Casq2*^{floxed} allele thus generated essentially is a wild-type *Casq2* allele but with *loxP* insertions at –561 bp and at +538 bp. In step 3, mice heterozygous for this *Casq2*^{floxed} allele were crossed with *EIIa-cre* transgenic females to remove *Casq2* sequences between the 2 *loxP* insertions, thus generating the *Casq2*$^{-}$ allele lacking the *Casq2* promoter, the entire first exon (431 bp encoding 78 amino acids), and 107 bp of intron 1. Finally, these *Casq2*$^{-}$ animals were twice backcrossed to C57BL/6 females to generate *Casq2*$^{-}$ heterozygotes lacking the *EIIa-cre* and *Rosa26-Flp* transgenes. These heterozygotes were intercrossed to generate all the animals used in this study. Genotyping assays are described in Supplemental Figure 1.

RNA analysis

RNA was isolated from 6- to 8-week-old mouse hearts using TriPure Isolation Reagent (Roche Applied Science). For quantitation of *Casq1* and *Casq2* expression, the RNA was converted to cDNA using the iScript cDNA Synthesis Kit (Bio-Rad) and analyzed by real-time PCR using LightCycler Fast-Start DNA Master SYBR Green I (Roche Applied Science) on the LightCycler Instrument (software package 5.32; Roche Applied Science). Primers for *Casq2* analysis were GCTGGAGGTCCAGGCCTTTGAG and GGCCACGATGTGGATCCCATTC, which target a 360-bp region starting in exon 4 and continuing to exon 8. Primers for the skeletal *Casq1* analysis were GATGCAGCTGTGGCCAAGAAAC and CATAGGCTCTTCCATGAAGGCC. RNA levels were standardized by comparison with expression of β-*microtubulin* using primers TGGTGCTTGTCTCACTGACC and GTCTCGATCCCAGTAGACGG.

To determine the structure of exon 1, total heart RNA was analyzed using the FirstChoice RLM-RACE kit (Ambion) using the *Casq2*-specific primers GGTTCGTGGTAATAGAGACAGA (inner primer) and CCAGTACAATCTCCTTCAGCT (outer primer). PCR products were cloned with the TOPO TA Cloning Kit (Invitrogen) and analyzed by restriction digestion and DNA sequencing.

Histology

Hearts from 10-week-old animals were fixed overnight in 4% paraformaldehyde buffered with 0.1 M sodium phosphate, pH 7.4; paraffin embedded; sectioned at 4 μm; stained with either H&E or Masson trichrome; and analyzed by a pathologist blinded to the genotype.

Echocardiography and ECG recordings and analysis

Surface ECG and echocardiography. For the surface ECG recording and echocardiography recordings were done as previously described (48, 49). Briefly, mice were anesthetized with isoflurane vapor titrated to maintain the lightest anesthesia possible. On average, 1.5% vol/vol isoflurane vapor was required to maintain adequate anesthesia. Loss of toe pinch reflex and respiration rate were used to monitor levels of anesthesia. Average respiration rate was not different between the 2 groups. Baseline ECG was recorded for 5 minutes, followed by an additional 20 minutes after i.p. administration of isoproterenol (1.5 mg/kg). The heart rate was measured as the average over a 30-second interval at baseline when a steady state was reached. All other ECG parameters (Supplemental Table 1) were measured manually after signal averaging for 10 seconds using a custom-built National Instruments LabVIEW program. Echocardiography parameters (Supplemental Table 1) were measured from 3 consecutive beats and averaged.

Telemetry. Mice were anesthetized (pentobarbital, 70 μg/g) before a transmitter (Data Sciences International) was placed into the abdominal cavity with subcutaneous electrodes in a lead 1 configuration. Animals were allowed to recover for at least 48 hours after surgery before participating in the treadmill exercise studies. As described previously (50), mice were placed individually into a special chamber of the motorized rodent treadmill (Exer-6M; Columbus Instruments) and exercised until they exhibited signs of exhaustion. Exhaustion was defined as the mouse spending more than 50% of the time or more than 15 seconds consecutively on the shock grid (51). Immediately after the shock grid was turned off, high-quality ECGs could be recorded. An analysis program (Dataquest A.R.T. version 2.3; Data Sciences International) was used to review the records and count PVCs, couplets, and runs of arrhythmias during the 10-minute period after exercise, as described previously (52).

Intracellular Ca^{2+} and myocyte shortening measurements

Myocyte isolation and Ca^{2+} indicator loading. Single ventricular myocytes were isolated by a modified collagenase/protease method as described previously (52). Our isolation procedure routinely yields 50%–70% rod-shaped, quiescent, and Ca^{2+}-tolerant ventricular myocytes. There was no difference in myocyte yield between the 2 groups of mice. All chemicals, unless otherwise specified, were obtained from Sigma-Aldrich. Ventricular myocytes were incubated with 2 μmol/l fura-2 acetoxymethyl ester (fura-2, AM; Invitrogen) for 8 minutes at room temperature to load the indicator in the cytosol. Myocytes were then washed twice for 10 minutes with Tyrode solution (TS) containing 250 μmol/l probenecid to retain the indicator in the cytosol. A minimum of 30 minutes was allowed for deesterification of the indicator before the cells were imaged. The composition of TS used for cell isolation and fura-2 loading was (in mmol/l): 145 NaCl, 5.4 KCl, 1.2 $CaCl_2$, 0.3 NaH_2PO_4, 0.5 $MgCl_2$, 5.5 glucose, and 5 HEPES, pH adjusted to 7.4 with NaOH. After fura-2 loading, all following experiments were conducted in TS containing a higher Ca concentration of 2 mmol/l.

Ca^{2+} fluorescence and myocyte shortening measurements. Fura-2–loaded healthy rod-shaped isolated ventricular myocytes were loaded in the experimental chamber, field stimulated, and superfused with TS. Intracellular

Ca^{2+} transients and myocyte shortening were simultaneously measured using a dual-beam excitation fluorescence photometry setup (IonOptix Corp.). After 5–10 minutes of steady-state pacing at 1 Hz, four 10-second-long Ca^{2+} fluorescence and shortening records were obtained for each myocyte. After that, myocytes were exposed for 4 seconds to TS containing 10 mmol/l caffeine and 20 mmol/l 2,3-butanedione monoxime using a rapid concentration-clamp system. The amplitude of the caffeine-induced Ca^{2+} transient was used as an estimate of total SR Ca^{2+} content (30). All experiments were conducted at room temperature (~23°C). Ca^{2+} transients and ventricular myocyte shortening were analyzed using specialized data analysis software (IonWizard; IonOptixCorp.). Excitation wavelengths of 360 and 380 nm were used to monitor the fluorescence signals of Ca^{2+}-bound and Ca^{2+}-free fura-2. After subtracting background and cellular autofluorescence, $[Ca^{2+}]_i$ is proportional to the fluorescence ratio at 360 nm and 380 nm excitation (53). Since fura-2/AM compartmentalizes into intracellular organelles (54), calculating intracellular Ca^{2+} concentrations from fura-2 fluorescence ratios can be problematic in intact cells. Thus, $[Ca^{2+}]_i$ measurements are reported as fluorescence ratios (F_{ratio}).

Analysis of spontaneous Ca^{2+} releases and Ca^{2+} oscillations. A spontaneous Ca^{2+} release was defined as any spontaneous increase of 0.07 ratiometric units or more from the diastolic F_{ratio} other than when triggered by field stimulation or caffeine. A Ca^{2+} oscillation was defined as any repetitive Ca^{2+} release faster than 5 Hz. Cells that displayed a specific event (spontaneous Ca^{2+} releases or Ca^{2+} oscillation) during the recording period were counted as positive and then expressed as percentage of total cells analyzed.

Protein analysis

Mouse ventricular homogenates and microsomes enriched in SR vesicles were prepared as described recently (55). SDS-PAGE and immunoblotting were conducted with the antibodies described in ref. 55. The anti-calsequestrin antibody used was raised to the cardiac protein and recognized both cardiac and skeletal muscle calsequestrins. Results of the Casq2 analysis were independently confirmed with a monoclonal antibody that recognizes residues 264–272 (downstream of the deletion) of Casq2. Antibody-binding protein bands were visualized with ^{125}I–protein A, then quantified with use of a Bio-Rad Personal FX phosphorimager. $^{45}Ca^{2+}$ overlay to detect Ca^{2+}-binding proteins in mouse SR vesicles was performed as described previously (11). Stains-all staining was done as described in ref. 5. Pure canine Casq2 was isolated by the phenyl-Sepharose method (3).

Electron microscopy

The hearts were fixed by perfusion through the left ventricle with 3.5% glutaraldehyde in 0.1 M sodium phosphate buffer, pH 7.2; kept at room temperature for 2 hours; and stored 4°C. Small bundles of cells teased either from the papillary muscles or from the walls of the left ventricle were postfixed in 2% OsO_4 in 0.1 M sodium cacodylate for 1 hour at room temperature, stained en bloc with saturated uranyl acetate in 70% EtOH, and embedded in Epon. Ultrathin sections (50–90 nm) were stained with saturated uranyl acetate solution in 50% ethanol and Sato lead solution (56). Sections were observed using a Philips 410 microscope (FEI Co.). Images were recorded either on film or using a Hamamatsu C4742-95 digital imaging system (Advanced Microscopy Techniques).

Estimates of relative surface areas and volumes of the total SR were obtained by the well-established stereology point and intersection counting techniques (57, 58) in digitally recorded images at a magnification of 42,000 from cross-sections of the cardiomyocytes, as detailed below; data for 1 mouse per group were obtained from the ventricular walls and for the other 2 from papillary muscles. Three or occasionally 2 micrographs covering a large portion of the cell cross-section were obtained for each cell in areas that excluded the nuclei and adjacent Golgi regions. The images were covered with an orthogonal array of dots at a spacing of 0.17 μm. The ratio of the numbers of dots falling over an organelle to the total number of dots covering the image gave the ratio of the organelle volume to the total volume. The number of dots covering the cytoplasm was obtained by subtracting mitochondrial from total dots. This ignored the small contribution of T tubules to the cytoplasmic area of the cell. In order to estimate surface area densities, the images were covered with 2 sets of grid lines separated by a distance of 0.24 μm and intersecting at right angles. The frequency of intersections between the membranes of the sectioned SR profiles and the grid lines was counted. The ratio of SR surface area to volume was obtained from the formula C/dP_{test}, where C is the number of intersections, d is the spacing between the grid lines, and P_{test} is the number of grid intersections in the test area.

Statistics

All experiments were done in random sequence with respect to the genotype, and measurements were taken by a single observer who was blinded to the genotype. Differences between groups were assessed using 1-way ANOVA. If statistically significant differences were found, individual groups were compared by 2-tailed Student's t test or nonparametric tests as indicated in the text. Results were considered statistically significant if the P value was less than 0.05. Unless otherwise indicated, results are expressed as mean ± SD.

Acknowledgments

This work was supported in part by NIH grants HL071670 (to B.C. Knollmann), HL46681 (to D.M. Roden and B.C. Knollmann), HL28556 (to L.R. Jones), and HL 48093 (to C. Franzini-Armstrong) and funds from the NICHD Intramural Research Program (to K. Pfeifer).

Received for publication May 18, 2006, and accepted in revised form July 11, 2006.

Address correspondence to: Björn C. Knollmann, Oates Institute for Experimental Therapeutics, Division of Clinical Pharmacology, Vanderbilt University Medical Center, 1265 Medical Research Building IV, Nashville, Tennessee 37232-0575, USA. Phone: (615) 343-6493; Fax: (615) 343-4522; E-mail: bjorn.knollmann@vanderbilt.edu.

1. Scott, B.T., Simmerman, H.K., Collins, J.H., Nadal-Ginard, B., and Jones, L.R. 1988. Complete amino acid sequence of canine cardiac calsequestrin deduced by cDNA cloning. *J. Biol. Chem.* **263**:8958–8964.
2. Yano, K., and Zarain-Herzberg, A. 1994. Sarcoplasmic reticulum calsequestrins: structural and functional properties. *Mol. Cell. Biochem.* **135**:61–70.
3. Cala, S.E., and Jones, L.R. 1983. Rapid purification of calsequestrin from cardiac and skeletal muscle sarcoplasmic reticulum vesicles by Ca2+-dependent elution from phenyl-sepharose. *J. Biol. Chem.* **258**:11932–11936.
4. Campbell, K.P., MacLennan, D.H., Jorgensen, A.O., and Mintzer, M.C. 1983. Purification and characterization of calsequestrin from canine cardiac sarcoplasmic reticulum and identification of the 53,000 dalton glycoprotein. *J. Biol. Chem.* **258**:1197–1204.
5. Jones, L.R., and Cala, S.E. 1981. Biochemical evidence for functional heterogeneity of cardiac sarcoplasmic reticulum vesicles. *J. Biol. Chem.* **256**:11809–11818.
6. Bers, D.M. 2002. Cardiac excitation-contraction coupling. *Nature.* **415**:198–205.
7. Franzini-Armstrong, C. 1980. Structure of sarcoplasmic reticulum. *Fed. Proc.* **39**:2403–2409.
8. Zhang, L., Kelley, J., Schmeisser, G., Kobayashi, Y.M., and Jones, L.R. 1997. Complex formation between junctin, triadin, calsequestrin, and the ryanodine receptor. Proteins of the cardiac junctional sarcoplasmic reticulum membrane. *J. Biol. Chem.* **272**:23389–23397.
9. Kobayashi, Y.M., and Jones, L.R. 1999. Identification of triadin 1 as the predominant triadin isoform expressed in mammalian myocardium. *J. Biol. Chem.* **274**:28660–28668.
10. Jones, L.R., Zhang, L., Sanborn, K., Jorgensen, A.O., and Kelley, J. 1995. Purification, primary structure, and immunological characterization of the 26-kDa calsequestrin binding protein (junctin) from

cardiac junctional sarcoplasmic reticulum. *J. Biol. Chem.* **270**:30787–30796.
11. Mitchell, R.D., Simmerman, H.K., and Jones, L.R. 1988. Ca2+ binding effects on protein conformation and protein interactions of canine cardiac calsequestrin. *J. Biol. Chem.* **263**:1376–1381.
12. Jones, L.R., et al. 1998. Regulation of Ca2+ signaling in transgenic mouse cardiac myocytes overexpressing calsequestrin. *J. Clin. Invest.* **101**:1385–1393.
13. Sato, Y., et al. 1998. Cardiac-specific overexpression of mouse cardiac calsequestrin is associated with depressed cardiovascular function and hypertrophy in transgenic mice. *J. Biol. Chem.* **273**:28470–28477.
14. Terentyev, D., et al. 2003. Calsequestrin determines the functional size and stability of cardiac intracellular calcium stores: mechanism for hereditary arrhythmia. *Proc. Natl. Acad. Sci. U. S. A.* **100**:11759–11764.
15. Miller, S.L., et al. 2005. Effects of calsequestrin over-expression on excitation-contraction coupling in isolated rabbit cardiomyocytes. *Cardiovasc. Res.* **67**:667–677.
16. Ikemoto, N., Ronjat, M., Meszaros, L.G., and Koshita, M. 1989. Postulated role of calsequestrin in the regulation of calcium release from sarcoplasmic reticulum. *Biochemistry.* **28**:6764–6771.
17. Gyorke, I., Hester, N., Jones, L.R., and Gyorke, S. 2004. The role of calsequestrin, triadin, and junctin in conferring cardiac ryanodine receptor responsiveness to luminal calcium. *Biophys. J.* **86**:2121–2128.
18. Zhang, L., Franzini-Armstrong, C., Ramesh, V., and Jones, L.R. 2001. Structural alterations in cardiac calcium release units resulting from overexpression of junctin. *J. Mol. Cell. Cardiol.* **33**:233–247.
19. Tijskens, P., Jones, L.R., and Franzini-Armstrong, C. 2003. Junctin and calsequestrin overexpression in cardiac muscle: the role of junctin and the synthetic and delivery pathways for the two proteins. *J. Mol. Cell. Cardiol.* **35**:961–974.
20. Takeshima, H., et al. 1998. Embryonic lethality and abnormal cardiac myocytes in mice lacking ryanodine receptor type 2. *EMBO J.* **17**:3309–3316.
21. Lahat, H., et al. 2001. A missense mutation in a highly conserved region of CASQ2 is associated with autosomal recessive catecholamine-induced polymorphic ventricular tachycardia in Bedouin families from Israel. *Am. J. Hum. Genet.* **69**:1378–1384.
22. Postma, A.V., et al. 2002. Absence of calsequestrin 2 causes severe forms of catecholaminergic polymorphic ventricular tachycardia. *Circ. Res.* **91**:e21–e26.
23. Terentyev, D., et al. 2006. Abnormal interactions of calsequestrin with the ryanodine receptor calcium release channel complex linked to exercise-induced sudden cardiac death. *Circ. Res.* **98**:1151–1158.
24. Priori, S.G., et al. 2002. Clinical and molecular characterization of patients with catecholaminergic polymorphic ventricular tachycardia. *Circulation.* **106**:69–74.
25. Priori, S.G., et al. 2001. Mutations in the cardiac ryanodine receptor gene (hRyR2) underlie catecholaminergic polymorphic ventricular tachycardia. *Circulation.* **103**:196–200.
26. Cala, S.E., Scott, B.T., and Jones, L.R. 1990. Intralumenal sarcoplasmic reticulum Ca(2+)-binding proteins. *Semin. Cell Biol.* **1**:265–275.
27. Cerrone, M., et al. 2005. Bidirectional ventricular tachycardia and fibrillation elicited in a knock-in mouse model carrier of a mutation in the cardiac ryanodine receptor. *Circ. Res.* **96**:e77–e82.
28. Leenhardt, A., et al. 1995. Catecholaminergic polymorphic ventricular tachycardia in children. A 7-year follow-up of 21 patients. *Circulation.* **91**:1512–1519.
29. Kort, A.A., Capogrossi, M.C., and Lakatta, E.G. 1985. Frequency, amplitude, and propagation velocity of spontaneous Ca++-dependent contractile waves in intact adult rat cardiac muscle and isolated myocytes. *Circ. Res.* **57**:844–855.
30. Bers, D.M. 2001. Sarcoplasmic reticulum. In *Excitation and contraction coupling and cardiac contractile force*. Kluwer Academic Publishers. Dordrecht, The Netherlands/Boston, Massachusetts, USA/London, United Kingdom. 161–202.
31. Bers, D.M. 2000. Calcium fluxes involved in control of cardiac myocyte contraction. *Circ. Res.* **87**:275–281.
32. Shannon, T.R., Ginsburg, K.S., and Bers, D.M. 2002. Quantitative assessment of the SR Ca2+ leak-load relationship. *Circ. Res.* **91**:594–600.
33. Page, E., Earley, J., and Power, B. 1974. Normal growth of ultrastructures in rat left ventricular myocardial cells. *Circ. Res.* **35**(Suppl. II):12–16.
34. Page, E., and McCallister, L.P. 1973. Quantitative electron microscopic description of heart muscle cells. Application to normal, hypertrophied and thyroxin-stimulated hearts. *Am. J. Cardiol.* **31**:172–181.
35. Xu, L., and Meissner, G. 1998. Regulation of cardiac muscle Ca2+ release channel by sarcoplasmic reticulum lumenal Ca2+. *Biophys. J.* **75**:2302–2312.
36. Marx, S.O., et al. 2000. PKA phosphorylation dissociates FKBP12.6 from the calcium release channel (ryanodine receptor): defective regulation in failing hearts. *Cell.* **101**:365–376.
37. Kohlhaas, M., et al. 2006. Increased sarcoplasmic reticulum calcium leak but unaltered contractility by acute CaMKII overexpression in isolated rabbit cardiac myocytes. *Circ. Res.* **98**:235–244.
38. Wang, W., Cleemann, L., Jones, L.R., and Morad, M. 2000. Modulation of focal and global Ca2+ release in calsequestrin-overexpressing mouse cardiomyocytes. *J. Physiol.* **524**:399–414.
39. Terentyev, D., et al. 2005. Triadin overexpression stimulates excitation-contraction coupling and increases predisposition to cellular arrhythmia in cardiac myocytes. *Circ. Res.* **96**:651–658.
40. Jiang, D., et al. 2004. RyR2 mutations linked to ventricular tachycardia and sudden death reduce the threshold for store-overload-induced Ca2+ release (SOICR). *Proc. Natl. Acad. Sci. U. S. A.* **101**:13062–13067.
41. Jiang, D., et al. 2005. Enhanced store overload-induced Ca2+ release and channel sensitivity to luminal Ca2+ activation are common defects of RyR2 mutations linked to ventricular tachycardia and sudden death. *Circ. Res.* **97**:1173–1181.
42. George, C.H., Higgs, G.V., and Lai, F.A. 2003. Ryanodine receptor mutations associated with stress-induced ventricular tachycardia mediate increased calcium release in stimulated cardiomyocytes. *Circ. Res.* **93**:531–540.
43. Wehrens, X.H., et al. 2003. FKBP12.6 deficiency and defective calcium release channel (ryanodine receptor) function linked to exercise-induced sudden cardiac death. *Cell.* **113**:829–840.
44. Lehnart, S.E., et al. 2004. Sudden death in familial polymorphic ventricular tachycardia associated with calcium release channel (ryanodine receptor) leak. *Circulation.* **109**:3208–3214.
45. Meissner, G. 1975. Isolation and characterization of two types of sarcoplasmic reticulum vesicles. *Biochim. Biophys. Acta.* **389**:51–68.
46. London, B. 2001. Cardiac arrhythmias: from (transgenic) mice to men. *J. Cardiovasc. Electrophysiol.* **12**:1089–1091.
47. Bers, D.M. 2001. Calcium sources and sinks. In *Excitation and contraction coupling and cardiac contractile force*. Kluwer Academic Publishers. Dordrecht, The Netherlands/Boston, Massachusetts, USA/London, United Kingdom. 39–56.
48. Knollmann, B.C., et al. 2001. Inotropic stimulation induces cardiac dysfunction in transgenic mice expressing a troponin T (I79N) mutation linked to familial hypertrophic cardiomyopathy. *J. Biol. Chem.* **276**:10039–10048.
49. Knollmann, B.C., Knollmann-Ritschel, B.E., Weissman, N.J., Jones, L.R., and Morad, M. 2000. Remodelling of ionic currents in hypertrophied and failing hearts of transgenic mice overexpressing calsequestrin. *J. Physiol.* **525**:483–498.
50. Hernandez, O.M., et al. 2005. F110I and R278C troponin T mutations that cause familial hypertrophic cardiomyopathy affect muscle contraction in transgenic mice and reconstituted human cardiac fibers. *J. Biol. Chem.* **280**:37183–37194.
51. Desai, K.H., et al. 1997. Cardiovascular indexes in the mouse at rest and with exercise: new tools to study models of cardiac disease. *Am. J. Physiol.* **272**:H1053–H1061.
52. Knollmann, B.C., et al. 2003. Familial hypertrophic cardiomyopathy-linked mutant troponin T causes stress-induced ventricular tachycardia and Ca2+-dependent action potential remodeling. *Circ. Res.* **92**:428–436.
53. Grynkiewicz, G., Poenie, M., and Tsien, R.Y. 1985. A new generation of Ca2+ indicators with greatly improved fluorescence properties. *J. Biol. Chem.* **260**:3440–3450.
54. Williford, D.J., Sharma, V.K., Korth, M., and Sheu, S.S. 1990. Spatial heterogeneity of intracellular Ca2+ concentration in nonbeating guinea pig ventricular myocytes. *Circ. Res.* **66**:241–248.
55. Kirchhefer, U., et al. 2004. Transgenic triadin 1 overexpression alters SR Ca2+ handling and leads to a blunted contractile response to beta-adrenergic agonists. *Cardiovasc. Res.* **62**:122–134.
56. Sato, T. 1968. A modified method for lead staining of thin sections. *J. Electron Microsc. (Tokyo).* **17**:158–159.
57. Loud, A.V., Barany, W.C., and Pack, B.A. 1965. Quantitative evaluation of cytoplasmic structures in electron micrographs. *Lab. Invest.* **14**:996–1008.
58. Mobley, B.A., and Eisenberg, B.R. 1975. Sizes of components in frog skeletal muscle measured by methods of stereology. *J. Gen. Physiol.* **66**:31–45.